





## Nonlinear magnetotransport in MoTe<sub>2</sub>

A. C. Marx <sup>\*</sup>, H. Jafari <sup>\*</sup>, E. K. Tekelenburg <sup>\*</sup>, M. A. Loi <sup>\*</sup>, J. Sławińska <sup>\*</sup>, and M. H. D. Guimarães <sup>†</sup>  
*Zernike Institute for Advanced Materials, University of Groningen, NL-9747AG Groningen, The Netherlands*



(Received 9 December 2023; accepted 7 February 2024; published 11 March 2024)

The shape of the Fermi surface influences many physical phenomena in materials and a growing interest in how the spin-dependent properties are related to the fermiology of crystals has surged. Recently, a novel current-dependent nonlinear magnetoresistance effect, known as bilinear magnetoelectric resistance (BMR), has been shown to be not only sensitive to the spin texture in spin-polarized nonmagnetic materials, but also dependent on the convexity of the Fermi surface in topological semimetals. In this paper, we show that the temperature dependence of the BMR signal strongly depends on the crystal axis of the semimetallic MoTe<sub>2</sub>. For the *a* axis, the amplitude of the signal remains fairly constant, while for the *b* axis it reverses sign at about 100 K. We calculate the BMR efficiencies at 10 K to be  $\chi_J^A = 173(3) \text{ nm}^2 \text{ T}^{-1} \text{ A}^{-1}$  and  $\chi_J^B = -364(13) \text{ nm}^2 \text{ T}^{-1} \text{ A}^{-1}$  for the *a* and *b* axis, respectively, and we find that they are comparable to the efficiencies measured for WTe<sub>2</sub>. We use density-functional theory calculations to compute the Fermi surfaces of both phases at different energy levels and we observe a change in convexity of the outermost electron pocket as a function of the Fermi energy. Our results suggest that the BMR signal is mostly dominated by the change in the Fermi-surface convexity.

DOI: [10.1103/PhysRevB.109.125408](https://doi.org/10.1103/PhysRevB.109.125408)

### I. INTRODUCTION

The bilinear magnetoelectric resistance (BMR) effect is a powerful technique to extract important information on the band structure of quantum materials, such as Fermi-surface convexity and spin textures [1–5]. The BMR effect causes a modulation of the material’s resistance depending on the relative angle between applied electric and magnetic fields [6]. This effect is also sometimes referred as the unidirectional magnetoresistance (UMR) [7,8] or electrical magnetochiral anisotropy [9–11] and, as the name suggests, it has a linear dependence with both current and magnetic field. The term UMR is also commonly used in the literature to address the effect in magnetic materials [12]. To avoid confusion, we will address this effect as BMR from now on. This effect has been used to explore the spin-dependent Fermi surface of systems with different electronic properties [1–3], and to give information on the shape and topology of the electron and hole pockets of semimetallic systems [4].

Weyl semimetals present an interesting platform to explore new physical phenomena due to their topologically protected states [13]. These states, called Fermi arcs, appear at the surface of materials and connect the conduction and valence band [14]. A lot of work has been done in understanding the influence of the topologically protected states on the transport properties of Weyl semimetals [15–21], but a complete understanding of the role of bulk bands is still lacking.

The Weyl semimetal candidate MoTe<sub>2</sub> is a van der Waals material showing low crystal symmetry [22–24] and strong spin-orbit coupling (SOC) [25,26]. Moreover, it undergoes

a crystallographic phase transition as a function of temperature [27]. MoTe<sub>2</sub> crystallizes in the monoclinic  $1T'$  phase at room temperature and transitions to the orthorhombic  $T_d$  phase below 240 K [27,28] [Fig. 1(a)]. The crystallographic lattice shows a metallic zigzag chain along the *b* axis, leading to a strong resistance anisotropy in the *ab* plane for both phases [28]. The phase transition also leads to a change on the crystal symmetry group, from space group  $P2_1/m$  to space group  $Pmn2_1$ , allowing for additional spintronic phenomena to occur [24,29,30]. It is important to note that  $1T'$ -MoTe<sub>2</sub> possesses inversion symmetry, which implies the absence of band splitting and thus, a zero net (bulk) spin texture. This results in a Fermi surface that is fully spin degenerate. However, a nonzero spin texture can appear at the surfaces, allowing for a “hidden” spin texture in the  $1T'$  phase [31–33]. Interestingly, the  $T_d$  phase is predicted to be a type-II Weyl state with two Weyl nodes close to the Fermi level, while the  $1T'$  phase remains a trivial semimetal [34–36]. Although a large magnetoresistance has been measured in  $T_d$ -MoTe<sub>2</sub> [15,37,38], the origins of the effect are not yet clear, since theoretical calculations indicate that MoTe<sub>2</sub> is an uncompensated semimetal [39]. Moreover, despite these interesting properties and promising spintronic [24,40–44] and topological applications [16–19,45,46], a study of its nonlinear magnetoresistance, i.e. the BMR effect, is lacking.

In this paper, we report on the BMR effect observed for the two main crystal axis of semimetallic MoTe<sub>2</sub> as a function of temperature. We observe a change in the BMR signal as we cool down from room temperature to 10 K which is strongly anisotropic with respect to the crystal axes (Fig. 1). For some of our devices we observe a crystal phase change as a function of temperature, which apparently is partially correlated to the change in the BMR signal. Despite this crystal phase change, density-functional theory (DFT) calculations show little changes on the overall band structure or band convexity

<sup>\*</sup>a.c.marx.goncalves@rug.nl

<sup>†</sup>m.h.guimaraes@rug.nl

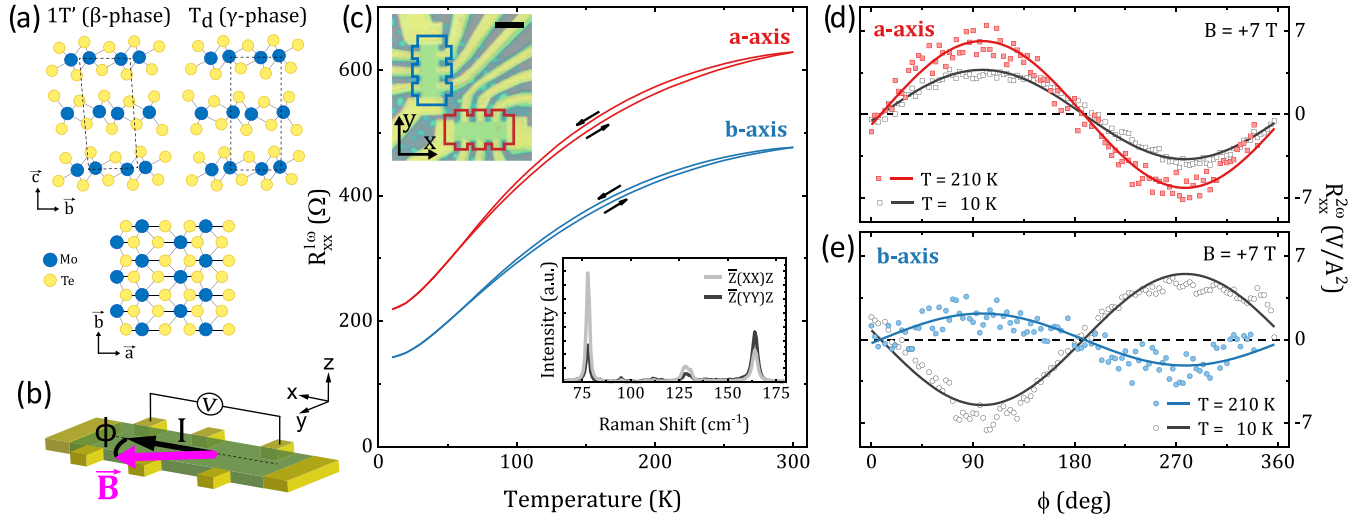


FIG. 1. (a) Crystal structure of semimetallic MoTe<sub>2</sub> in the 1T' and T<sub>d</sub> crystal phases. (b) Schematics for the bilinear magnetoelectric resistance measurements. (c) Longitudinal resistance as a function of temperature measured with the current along the two main crystal axes of MoTe<sub>2</sub>. The top inset shows an optical image of the device (scale bar corresponds to 5 μm) and the bottom inset shows the polarized Raman spectra for each axis. BMR measurements with the current applied along the *a* (d) and *b* axis (e) with an in-plane magnetic field of 7 T for two different temperatures (10 and 210 K). A vertical offset was removed for clarity.

at the Fermi level for both phases. This indicates that the strong dependence of the BMR signal we observe could be attributed to a change on the Fermi-surface convexity resulting from a Fermi level shift as a function of temperature, as observed in the sister material T<sub>d</sub>-WTe<sub>2</sub> [4].

## II. RESULTS AND DISCUSSION

Our devices consist of 1T'-MoTe<sub>2</sub> encapsulated in hexagonal boron nitride (hBN), fabricated by mechanically exfoliated crystals (HQ Graphene), and stacked on top of each other via a dry van der Waals assembly technique [47]. The hBN/1T'-MoTe<sub>2</sub>/hBN stack is assembled and placed on a SiO<sub>2</sub>/Si substrate under a nitrogen environment to protect the MoTe<sub>2</sub> crystals from degrading. Two perpendicular Hall bars were patterned on the stack, on the same MoTe<sub>2</sub> flake, using electron-beam lithography and followed by Ti/Au contact deposition by conventional techniques. The channel of each Hall bar was designed to be aligned with one of the main axes of the crystal. The measurements were performed using conventional harmonic low-frequency (177 Hz) lock-in techniques with current biases below  $I_0 = 500 \mu\text{A}$  in a variable-temperature insert in helium gas. The in-plane angle ( $\phi$ ) between an external magnetic field (up to  $B = 7 \text{ T}$ ) and the current direction was varied while measuring the second-harmonic voltage in the longitudinal direction [Fig. 1(b)]. The measurements for the transverse direction can be found in the Supplemental Material [48]. We have measured three different sets of devices with different MoTe<sub>2</sub> thicknesses ( $t$ ). The change in the BMR signal as a function of temperature is clearly observed in two of our samples,  $t = 6$  and 12 nm. Here, we report our findings on the sample with  $t = 12$  nm as obtained by atomic force microscopy. More details on the device fabrication and the results for other samples can be found in the Supplemental Material [48].

The complete device is shown in the top inset of Fig. 1(c), outlining each Hall bar with different colors to indicate

the alignment of the channel with the *a* (red) and *b* axis (blue). To confirm this alignment we performed polarized Raman spectroscopy measurements [49–51] [bottom inset of Fig. 1(c)] and further characterized our sample by measuring the longitudinal (first-harmonic) resistance as function of temperature, as shown in Fig. 1(c). As expected, a clear resistance anisotropy is observed between the two axes, where the low-resistive *b* axis is along the metallic chain. Moreover, a small hysteresis loop appears in the interval between 80 and 300 K as the sample is cooled down and warmed up again. This behavior has been observed in thin MoTe<sub>2</sub> flakes and confirmed to be due to a phase transition from the 1T' to the T<sub>d</sub> phase. Different than for bulk MoTe<sub>2</sub> this phase transition is not abrupt, resulting from a coexistence of the two phases, with the main crystal phase changing between the 1T' and the T<sub>d</sub> phases with temperature [52,53].

The BMR effect arises from the interplay between the applied current and magnetic field. Mathematically, we can express the resistance of a material by a resistance term  $R_0$ , plus a term linear on the current and magnetic field:  $IR_1(\mathbf{B})$ . For an ac-current  $I = I_0 \sin(\omega t)$  applied through the material, therefore, the longitudinal voltage can be easily written by Ohm's law, yielding

$$V = R_0 I_0 \sin(\omega t) + \frac{1}{2} R_1 I_0^2 + \frac{1}{2} R_1 I_0^2 \sin\left(2\omega t - \frac{\pi}{2}\right), \quad (1)$$

with the first-harmonic, dc, and second-harmonic components of the longitudinal voltage signal being the first, second, and third terms on the right, respectively. As can be seen, both dc and  $V_{xx}^{2\omega}$  are proportional to the BMR coefficient  $R_1$ . Here, we focus on the second-harmonic response, which is less prone to additional artifacts.

We observe a remarkably different behavior on the second-harmonic longitudinal resistance ( $R_{xx}^{2\omega}$ ) as a function of temperature for the two crystal axes. Here, we define

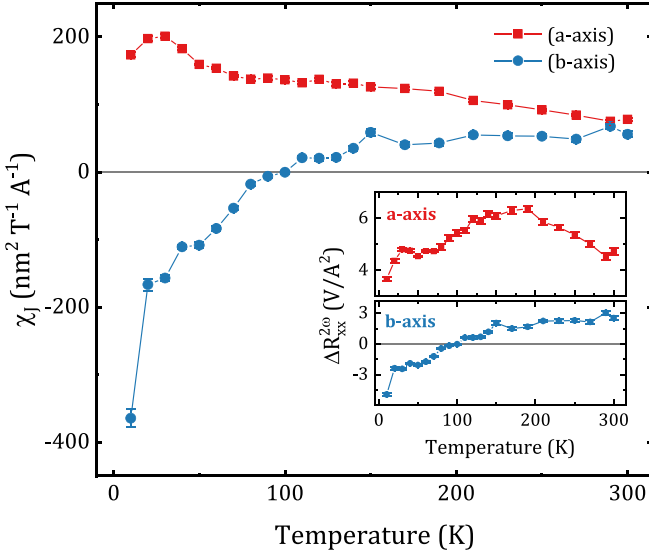


FIG. 2. The efficiency  $\chi_J$  for the current applied along the  $a$  and  $b$  axis as a function of temperature. The inset shows the amplitude  $\Delta R_{xx}^{2\omega}$  of the fittings for the second-harmonic resistance measurements.

$R_{xx}^{2\omega} = \frac{V_{xx}^{2\omega}}{(I_0)^2}$ . Figures 1(d) and 1(e) show the results for  $I_0$  parallel to the  $a$  and  $b$  axis, respectively, for a magnetic field of +7 T and two different temperatures (10 and 210 K). Experimental data are represented by the scattered points, while the solid lines are the corresponding fits according to

$$R_{xx}^{2\omega} = \Delta R_{xx}^{2\omega} \sin[2(\phi + \phi_0)] + y_0, \quad (2)$$

where  $\Delta R_{xx}^{2\omega}$  is the amplitude of the signal, and  $\phi_0$  and  $y_0$  are the angular and vertical offsets, respectively. For both axes we notice that  $R_{xx}^{2\omega}$  shows a sinusoidal behavior with a periodicity of  $2\pi$ . Regions of high- and low-resistance states can be found at angles of about  $90^\circ$  and  $180^\circ$ . This agrees with a picture of a BMR signal arising from a Rashba-like spin texture for the Fermi surface of MoTe<sub>2</sub>. Strikingly, the two axes show very different behaviors as the temperature is reduced. For the  $a$  axis, we observe only a small difference between the amplitudes at 10 and 210 K, while for the  $b$  axis the amplitude is not only  $\sim 2.5$  times larger at 10 K, but it also changes sign compared to the measurement at 210 K. Further characterization of our signals, showing the magnetic field and current dependence of  $R_{xx}^{2\omega}$  for both  $a$  and  $b$  axis can be found in the Supplemental Material [48]. In order to elucidate the origins of the different behavior for the two crystal axes, we perform similar measurements at various temperatures (inset of Fig. 2). Interestingly,  $\Delta R_{xx}^{2\omega}$  remains fairly constant for the  $a$  axis, while for the  $b$  axis the amplitude goes from positive to negative as the temperature decreases. We note that  $\Delta R_{xx}^{2\omega}$  can strongly depend on the specific device geometry and on the temperature dependence of the resistivity. In order to exclude such effects, we calculate the BMR efficiency, defined as

$$\chi_J = \frac{2\Delta R_{xx}^{2\omega} w t}{R_0 B}, \quad (3)$$

with  $w$  being the channel width. The values for the BMR efficiency as a function of temperature are plotted in Fig. 2.

We see that  $\chi_J$  reaches similar and positive values for both the  $a$  and  $b$  axes at high temperatures. Since a spin-dependent BMR signal is not expected at the  $1T'$  phase, a discussion on the potential causes for the observed BMR signals can be found in the Supplemental Material [48] (see also Ref. [54] therein). As the temperature decreases, the BMR efficiency increases modestly for the  $a$  axis, peaking around 30 K. Differently,  $\chi_J$  decreases drastically for the  $b$  axis, crossing zero at around 100 K. Cooling down further, the BMR efficiency drops rapidly for the  $b$  axis and at 10 K we obtain a BMR magnitude of twice as large as the one for the  $a$  axis. The computed values are  $\chi_J^A = 173(3) \text{ nm}^2 \text{ T}^{-1} \text{ A}^{-1}$  and  $\chi_J^B = -364(13) \text{ nm}^2 \text{ T}^{-1} \text{ A}^{-1}$  for the  $a$  and  $b$  axes, respectively. These values and temperature behavior are comparable to the ones reported for the sister material WTe<sub>2</sub> [4]. However, we point out that different from MoTe<sub>2</sub>, WTe<sub>2</sub> does not undergo a crystal phase transition with a change in temperature. The results for WTe<sub>2</sub> were explained as a change in the convexity of the electron pockets as a function of the Fermi level [4]. Nonetheless, it is known that BMR can also depend on the spin texture of the Fermi surfaces [1–3].

To further understand the origins of the behavior we observe, we performed DFT calculations to compute the Fermi contours of the hole and electron bands at different Fermi levels and for both crystal phases. Details of the calculations can be found in the Supplemental Material [48] (see also Refs. [55–62] therein). As shown in Fig. 3(a), the overall electronic dispersion presents some similar features for both  $1T'$  and  $T_d$  phases. Both show a semimetallic behavior, with electron and hole pockets at the Fermi level. Due to the presence of inversion symmetry in the  $1T'$  phase, we do not see any spin splitting in the DFT calculations. However, the  $T_d$  lacks inversion symmetry and shows a Rashba-like spin texture, i.e., with the spins perpendicular to the crystal momentum (see Supplemental Material [48] for the spin-dependent electronic dispersion). For this reason, we rule out that the BMR signal is dominated by a spin-dependent contribution, since the second-harmonic signal reverses sign with temperature which would imply a reversal on the spin direction.

Similar to WTe<sub>2</sub>, it has been demonstrated that MoTe<sub>2</sub> can show a shift on the Fermi level as a function of temperature [63–66]. To explore the implications of this to our measurements, we obtain the Fermi surfaces at different energies (Fig. 3) for both phases. The overall behavior of the electron and hole pockets with the change in energy is similar for both  $1T'$ - and  $T_d$ -MoTe<sub>2</sub>, however, the latter shows two extra hole pockets appearing at low energies. Remarkably, we obtain a change in convexity of the electron pockets for both phases along the  $\Gamma$ - $Y$  direction. This change in convexity is consistent with the sign change we observe in our measurements, revealing that our measurements are dominated by a change in the Fermi-surface convexity.

### III. CONCLUSION

Our observations of a BMR signal dominated by the Fermi-surface convexity in MoTe<sub>2</sub> are an important step for the understanding of the band structure of this Weyl semimetal candidate. Here, we report an anisotropic behavior of the

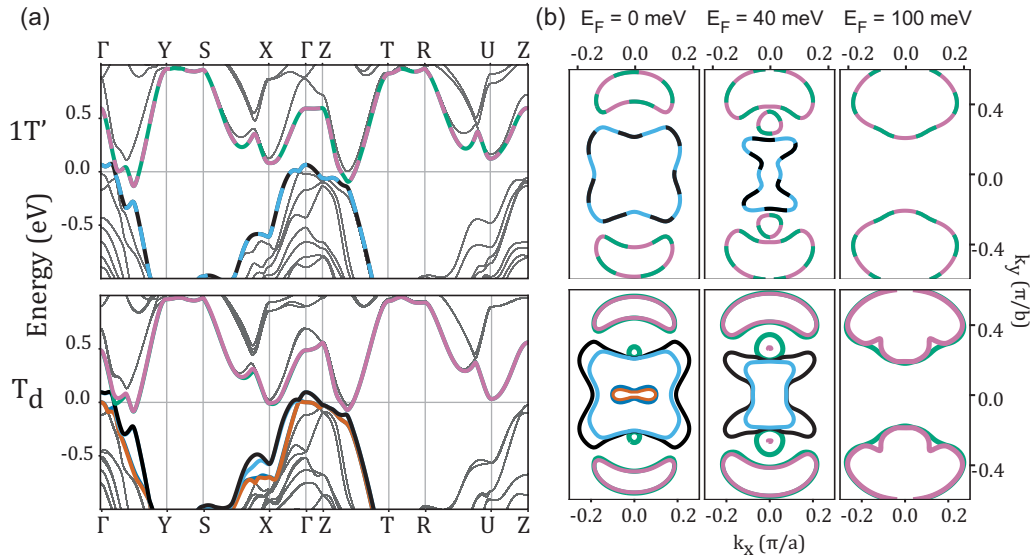


FIG. 3. (a) Electronic dispersion for the  $1T'$  and  $T_d$  phases, and (b) corresponding Fermi surfaces at different energy cuts in respect to the conduction bands:  $E_F = 0, 40,$  and  $100$  meV. For the bands (and corresponding Fermi surfaces) of the  $1T'$  phase, the mixing of two colors represents the spin degenerate bands.

BMR signal as a function of temperature, with a clear inversion below 100 K for the current along the  $b$  axis while no sign reversal is observed for the current along the  $a$  axis. This observation is in agreement with a change in the Fermi-surface convexity, induced by a change in the Fermi level due to temperature, similar to what has been reported for the sister material  $WTe_2$  [4]. We envision that our demonstration of large BMR signals in  $MoTe_2$  can be exploited in spintronic devices consisting of  $MoTe_2$  interfaced with two-dimensional magnets, for which the magnetic field role could be played by the magnetic exchange. This would allow one to obtain important information on the magnetization direction even on magnetic insulators, while also exploiting the unusual spin-torque symmetries [24] provided by  $MoTe_2$  for magnetization manipulation.

The raw data and the data underlying the figures in the main text are publicly available through the data repository Zenodo [67].

#### ACKNOWLEDGMENTS

We thank T. Liu for the valuable knowledge shared on measurements and sample fabrication. We thank J. G. Holstein, H. Adema, H. de Vries, A. Joshua, and F. H. van der Velde for their technical support. This work was supported by the Dutch Research Council (NWO) through Grant No. STU.019.014, the Zernike Institute for Advanced Materials, the research program “Materials for the Quantum Age” (QuMat, Registration No. 024.005.006), which is part of the Gravitation program financed by the Dutch Ministry of Education, Culture and Science (OCW), and the European Union (ERC, 2DOPTOSPIN, 101076932). Views and opinions expressed are however those of the author(s) only and do not necessarily reflect those of the European Union or the European Research Council. Neither the European Union nor the granting authority can be held responsible for them. The device fabrication and nanocharacterization were performed using Zernike NanoLabNL facilities.

- [1] P. He, S. S.-L. Zhang, D. Zhu, Y. Liu, Y. Wang, J. Yu, G. Vignale, and H. Yang, *Nat. Phys.* **14**, 495 (2018).
- [2] P. He, S. M. Walker, S. S.-L. Zhang, F. Y. Bruno, M. S. Bahramy, J. M. Lee, R. Ramaswamy, K. Cai, O. Heinonen, G. Vignale, F. Baumberger, and H. Yang, *Phys. Rev. Lett.* **120**, 266802 (2018).
- [3] Y. Zhang, V. Kalappattil, C. Liu, M. Mehraeen, S. S.-L. Zhang, J. Ding, U. Erugu, Z. Chen, J. Tian, K. Liu, J. Tang, and M. Wu, *Sci. Adv.* **8**, eabo0052 (2022).
- [4] P. He, C.-H. Hsu, S. Shi, K. Cai, J. Wang, Q. Wang, G. Eda, H. Lin, V. M. Pereira, and H. Yang, *Nat. Commun.* **10**, 1290 (2019).
- [5] T. Liu, A. Roy, J. Hidding, H. Jafari, D. K. de Wal, J. Sławińska, M. H. D. Guimarães, and B. J. van Wees, *Phys. Rev. B* **108**, 165407 (2023).
- [6] S. S.-L. Zhang and G. Vignale, *Proc. SPIE* **10732**, 1073215 (2018).
- [7] T. Guillet, C. Zucchetti, Q. Barbedienne, A. Marty, G. Isella, L. Cagnon, C. Vergnaud, H. Jaffrès, N. Reyren, J.-M. George, A. Fert, and M. Jamet, *Phys. Rev. Lett.* **124**, 027201 (2020).
- [8] F. Calavalle, M. Suárez-Rodríguez, B. Martín-García, A. Johansson, D. C. Vaz, H. Yang, I. V. Maznichenko, S. Ostanin, A. Mateo-Alonso, A. Chuvilin, I. Mertig, M. Gobbi, F. Casanova, and L. E. Hueso, *Nat. Mater.* **21**, 526 (2022).



- [9] G. L. J. A. Rikken, J. Fölling, and P. Wyder, *Phys. Rev. Lett.* **87**, 236602 (2001).
- [10] Y. Wang, H. F. Legg, T. Bömerich, J. Park, S. Biesenkamp, A. A. Taskin, M. Braden, A. Rosch, and Y. Ando, *Phys. Rev. Lett.* **128**, 176602 (2022).
- [11] T. Yokouchi, Y. Ikeda, T. Morimoto, and Y. Shiomi, *Phys. Rev. Lett.* **130**, 136301 (2023).
- [12] C. O. Avci, K. Garello, A. Ghosh, M. Gabureac, S. F. Alvarado, and P. Gambardella, *Nat. Phys.* **11**, 570 (2015).
- [13] A. A. Burkov, *Nat. Mater.* **15**, 1145 (2016).
- [14] K. Deng, G. Wan, P. Deng, K. Zhang, S. Ding, E. Wang, M. Yan, H. Huang, H. Zhang, Z. Xu, J. Denlinger, A. Fedorov, H. Yang, W. Duan, H. Yao, Y. Wu, S. Fan, H. Zhang, X. Chen, and S. Zhou, *Nat. Phys.* **12**, 1105 (2016).
- [15] F. C. Chen, H. Y. Lv, X. Luo, W. J. Lu, Q. L. Pei, G. T. Lin, Y. Y. Han, X. B. Zhu, W. H. Song, and Y. P. Sun, *Phys. Rev. B* **94**, 235154 (2016).
- [16] X. Qian, J. Liu, L. Fu, and J. Li, *Science* **346**, 1344 (2014).
- [17] Y. Zhang, J. van den Brink, C. Felser, and B. Yan, *2D Mater.* **5**, 044001 (2018).
- [18] F. C. Chen, X. Luo, J. Yan, Y. Sun, H. Y. Lv, W. J. Lu, C. Y. Xi, P. Tong, Z. G. Sheng, X. B. Zhu, W. H. Song, and Y. P. Sun, *Phys. Rev. B* **98**, 041114(R) (2018).
- [19] Y. Zhang, Y. Sun, and B. Yan, *Phys. Rev. B* **97**, 041101(R) (2018).
- [20] S. Khim, K. Koepernik, D. V. Efremov, J. Klotz, T. Förster, J. Wosnitza, M. I. Sturza, S. Wurmehl, C. Hess, J. van den Brink, and B. Büchner, *Phys. Rev. B* **94**, 165145 (2016).
- [21] G. Sharma, P. Goswami, and S. Tewari, *Phys. Rev. B* **96**, 045112 (2017).
- [22] K. Zhang, C. Bao, Q. Gu, X. Ren, H. Zhang, K. Deng, Y. Wu, Y. Li, J. Feng, and S. Zhou, *Nat. Commun.* **7**, 13552 (2016).
- [23] S.-Y. Chen, T. Goldstein, D. Venkataraman, A. Ramasubramaniam, and J. Yan, *Nano Lett.* **16**, 5852 (2016).
- [24] G. M. Stiehl, R. Li, V. Gupta, I. E. Baggari, S. Jiang, H. Xie, L. F. Kourkoutis, K. F. Mak, J. Shan, R. A. Buhrman, and D. C. Ralph, *Phys. Rev. B* **100**, 184402 (2019).
- [25] C. H. Naylor, W. M. Parkin, J. Ping, Z. Gao, Y. R. Zhou, Y. Kim, F. Streller, R. W. Carpick, A. M. Rappe, M. Drndić, J. M. Kikkawa, and A. T. C. Johnson, *Nano Lett.* **16**, 4297 (2016).
- [26] J. Cui, P. Li, J. Zhou, W.-Y. He, X. Huang, J. Yi, J. Fan, Z. Ji, X. Jing, F. Qu, Z. G. Cheng, C. Yang, L. Lu, K. Suenaga, J. Liu, K. T. Law, J. Lin, Z. Liu, and G. Liu, *Nat. Commun.* **10**, 2044 (2019).
- [27] R. Clarke, E. Marseglia, and H. P. Hughes, *Philos. Mag.* **B 38**, 121 (1978).
- [28] H. P. Hughes and R. H. Friend, *J. Phys. C: Solid State Phys.* **11**, L103 (1978).
- [29] A. Roy, M. H. D. Guimarães, and J. Sławińska, *Phys. Rev. Mater.* **6**, 045004 (2022).
- [30] K. Tenzin, A. Roy, H. Jafari, B. Banas, F. T. Cerasoli, M. Date, A. Jayaraj, M. Buongiorno Nardelli, and J. Sławińska, *Phys. Rev. B* **107**, 165140 (2023).
- [31] Q. Liu, X. Zhang, and A. Zunger, *Phys. Rev. Lett.* **114**, 087402 (2015).
- [32] H. Yuan, M. S. Bahramy, K. Morimoto, S. Wu, K. Nomura, B.-J. Yang, H. Shimotani, R. Suzuki, M. Toh, C. Kloc, X. Xu, R. Arita, N. Nagaosa, and Y. Iwasa, *Nat. Phys.* **9**, 563 (2013).
- [33] J. M. Riley, F. Mazzola, M. Dendzik, M. Michiardi, T. Takayama, L. Bawden, C. Granerød, M. Leandersson, T. Balasubramanian, M. Hoesch, T. K. Kim, H. Takagi, W. Meevasana, Ph. Hofmann, M. S. Bahramy, J. W. Wells, and P. D. C. King, *Nat. Phys.* **10**, 835 (2014).
- [34] Y. Sun, S.-C. Wu, M. N. Ali, C. Felser, and B. Yan, *Phys. Rev. B* **92**, 161107(R) (2015).
- [35] Z. Wang, D. Gresch, A. A. Soluyanov, W. Xie, S. Kushwaha, X. Dai, M. Troyer, R. J. Cava, and B. A. Bernevig, *Phys. Rev. Lett.* **117**, 056805 (2016).
- [36] J. Jiang, Z. Liu, Y. Sun, H. Yang, C. Rajamathi, Y. Qi, L. Yang, C. Chen, H. Peng, C.-C. Hwang, S. Sun, S.-K. Mo, I. Vobornik, J. Fujii, S. Parkin, C. Felser, B. Yan, and Y. Chen, *Nat. Commun.* **8**, 13973 (2017).
- [37] S. Lee, J. Jang, S.-I. Kim, S.-G. Jung, J. Kim, S. Cho, S. W. Kim, J. Y. Rhee, K.-S. Park, and T. Park, *Sci. Rep.* **8**, 13937 (2018).
- [38] Q. L. Pei, W. J. Meng, X. Luo, H. Y. Lv, F. C. Chen, W. J. Lu, Y. Y. Han, P. Tong, W. H. Song, Y. B. Hou, Q. Y. Lu, and Y. P. Sun, *Phys. Rev. B* **96**, 075132 (2017).
- [39] S. Thirupathiah, R. Jha, B. Pal, J. S. Matias, P. K. Das, P. K. Sivakumar, I. Vobornik, N. C. Plumb, M. Shi, R. A. Ribeiro, and D. D. Sarma, *Phys. Rev. B* **95**, 241105(R) (2017).
- [40] S. Lim, C. R. Rajamathi, V. Süß, C. Felser, and A. Kapitulnik, *Phys. Rev. B* **98**, 121301(R) (2018).
- [41] C. K. Safeer, N. Ontoso, J. Ingla-Aynés, F. Herling, V. T. Pham, A. Kurzman, K. Ensslin, A. Chuvilin, I. Robredo, M. G. Vergniory, F. De Juan, L. E. Hueso, M. R. Calvo, and F. Casanova, *Nano Lett.* **19**, 8758 (2019).
- [42] J. Zhou, J. Qiao, A. Bournel, and W. Zhao, *Phys. Rev. B* **99**, 060408(R) (2019).
- [43] N. Ontoso, C. K. Safeer, F. Herling, J. Ingla-Aynés, H. Yang, Z. Chi, B. Martin-Garcia, I. Robredo, M. G. Vergniory, F. de Juan, M. Reyes Calvo, L. E. Hueso, and F. Casanova, *Phys. Rev. Appl.* **19**, 014053 (2023).
- [44] A. M. Hoque, D. Khokhriakov, K. Zollner, B. Zhao, B. Karpiak, J. Fabian, and S. P. Dash, *Commun. Phys.* **4**, 124 (2021).
- [45] X. Luo, F. C. Chen, J. L. Zhang, Q. L. Pei, G. T. Lin, W. J. Lu, Y. Y. Han, C. Y. Xi, W. H. Song, and Y. P. Sun, *Appl. Phys. Lett.* **109**, 102601 (2016).
- [46] S. Singh, J. Kim, K. M. Rabe, and D. Vanderbilt, *Phys. Rev. Lett.* **125**, 046402 (2020).
- [47] P. J. Zomer, M. H. D. Guimarães, J. C. Brant, N. Tombros, and B. J. van Wees, *Appl. Phys. Lett.* **105**, 013101 (2014).
- [48] See Supplemental Material at <http://link.aps.org/supplemental/10.1103/PhysRevB.109.125408> for the data of the transverse resistance of the sample showed in the main text; details on the device fabrication and results on other samples; the BMR characterization with magnetic field and current dependence; a discussion on the potential causes for the observed BMR signal at room temperature; and details of the DFT calculations, which includes Refs. [4,22,23,47,49–51,53].
- [49] L. Zhou, S. Huang, Y. Tatsumi, L. Wu, H. Guo, Y.-Q. Bie, K. Ueno, T. Yang, Y. Zhu, J. Kong, R. Saito, and M. Dresselhaus, *J. Am. Chem. Soc.* **139**, 8396 (2017).
- [50] J. Wang, X. Luo, S. Li, I. Verzhbitskiy, W. Zhao, S. Wang, S. Y. Quek, and G. Eda, *Adv. Funct. Mater.* **27**, 1604799 (2017).
- [51] Q. Song, H. Wang, X. Pan, X. Xu, Y. Wang, Y. Li, F. Song, X. Wan, Y. Ye, and L. Dai, *Sci. Rep.* **7**, 1758 (2017).

- [52] R. He, S. Zhong, H. H. Kim, G. Ye, Z. Ye, L. Winford, D. McHaffie, I. Rilak, F. Chen, X. Luo, Y. Sun, and A. W. Tsen, *Phys. Rev. B* **97**, 041410(R) (2018).
- [53] Y. Cheon, S. Y. Lim, K. Kim, and H. Cheong, *ACS Nano* **15**, 2962 (2021).
- [54] R. Beams, L. G. Cançado, S. Krylyuk, I. Kalish, B. Kalanyan, A. K. Singh, K. Choudhary, A. Bruma, P. M. Vora, F. Tavazza, A. V. Davydov, and S. J. Stranick, *ACS Nano* **10**, 9626 (2016).
- [55] P. Giannozzi, S. Baroni, N. Bonini, M. Calandra, R. Car, C. Cavazzoni, D. Ceresoli, G. L. Chiarotti, M. Cococcioni, I. Dabo *et al.*, *J. Phys.: Condens. Matter* **21**, 395502 (2009).
- [56] P. Giannozzi Jr, O. Andreussi, T. Brumme, O. Bunau, M. Buongiorno Nardelli, M. Calandra, R. Car, C. Cavazzoni, D. Ceresoli, M. Cococcioni, N. Colonna, I. Carnimeo, A. Dal Corso, S. De Gironcoli, P. Delugas, R. A. DiStasio, Jr., A. Ferretti, A. Floris, G. Fratesi, G. Fugallo *et al.*, *J. Phys.: Condens. Matter* **29**, 465901 (2017).
- [57] G. Kresse and J. Furthmüller, *Comput. Mater. Sci.* **6**, 15 (1996).
- [58] P. E. Blöchl, *Phys. Rev. B* **50**, 17953 (1994).
- [59] S. Grimme, J. Antony, S. Ehrlich, and H. Krieg, *J. Chem. Phys.* **132**, 154104 (2010).
- [60] J. P. Perdew, K. Burke, and M. Ernzerhof, *Phys. Rev. Lett.* **77**, 3865 (1996).
- [61] M. Buongiorno Nardelli, F. T. Cerasoli, M. Costa, S. Curtarolo, R. D. Gennaro, M. Fornari, L. Liyanage, A. R. Supka, and H. Wang, *Comput. Mater. Sci.* **143**, 462 (2018).
- [62] F. T. Cerasoli, A. R. Supka, A. Jayaraj, M. Costa, I. Siloi, J. Sławińska, S. Curtarolo, M. Fornari, D. Ceresoli, and M. Buongiorno Nardelli, *Comput. Mater. Sci.* **200**, 110828 (2021).
- [63] Y. Wu, N. H. Jo, M. Ochi, L. Huang, D. Mou, S. L. Bud'ko, P. C. Canfield, N. Trivedi, R. Arita, and A. Kaminski, *Phys. Rev. Lett.* **115**, 166602 (2015).
- [64] N. Xu, Z. W. Wang, A. Magrez, P. Bugnon, H. Berger, C. E. Matt, V. N. Strocov, N. C. Plumb, M. Radovic, E. Pomjakushina, K. Conder, J. H. Dil, J. Mesot, R. Yu, H. Ding, and M. Shi, *Phys. Rev. Lett.* **121**, 136401 (2018).
- [65] S. Beaulieu, S. Dong, N. Tancogne-Dejean, M. Dendzik, T. Pincelli, J. Maklar, R. P. Xian, M. A. Sentef, M. Wolf, A. Rubio, L. Rettig, and R. Ernstorfer, *Sci. Adv.* **7**, eabd9275 (2021).
- [66] D. Kim, J.-H. Lee, K. Kang, D. Won, M. Kwon, S. Cho, Y.-W. Son, and H. Yang, *Adv. Electron. Mater.* **7**, 2000823 (2021).
- [67] A. C. Marx, H. Jafari, E. K. Tekelenburg, M. A. Loi, J. Sławińska, and M. H. D. Guimarães, Dataset of “Nonlinear magnetotransport in MoTe<sub>2</sub>” (Version v1), Zenodo (2024), <https://doi.org/10.5281/zenodo.10592551>.